Evaluation of the Micro-Angiographic Fluoroscope as a High-Resolution, Single-Photon Counting and Energy-Integrating Imager for Transmission and Emission Imaging

Amit Jain, Ashish Panse, Daniel. R. Bednarek, Rutao Yao, *Member, IEEE*, and S. Rudin, *Life Member, IEEE*

***Abstract*—X-ray and radionuclide imaging are widely popular medical imaging modalities. The requirements for each imaging modality are different, and different detectors are normally used. For this paper, we demonstrate our new detector capable of both fluoroscopy and angiography, to be used as an imager for both single-photon and integral-energy imaging and applied to the dual modalities of radionuclide imaging and X-ray imaging. This newly developed micro-angiographic fluoroscope (MAF) has 1024 × 1024 pixels of 35 μm effective size and is capable of real-time imaging at 30 fps. The large variable gain of its light image intensifier (LII) provides quantum-limited operation with essentially no additive instrumentation noise. We demonstrate that the MAF can be operated in single-photon counting (SPC) mode for X-ray imaging with substantially better resolution than in energy integration (EI) mode. We may use high LII gain with very low exposure (less than 1 X-ray photon/pixel) per frame for SPC mode (with X-ray and radionuclide) and higher exposure with lower gain for EI mode (transmission imaging with X-rays). For a demonstration of the operation in both EI and SPC mode, a heavily K-edge filtered X-ray beam (average energy of 31 keV) was used to provide a nearly monochromatic spectrum. The MTF measured using a standard slit method showed a dramatic improvement for the SPC mode over the EI mode at all spatial frequencies. Images of a line-pair phantom also showed improved spatial resolution in SPC mode compared to EI mode. In SPC mode, images of human distal and middle phalanges showed the trabecular structures of the bone with far better contrast and detail. We also show MAF operation in SPC mode for radionuclide imaging using a custom-built phantom filled with I-125. A 1-mm-diameter parallel hole, medium-energy gamma camera collimator was placed between the phantom, and the MAF and was moved multiple times at equal intervals in random directions to eliminate the pattern corresponding to the collimator septa. Data was acquired at 20 fps, and multiple signal-thresholded frames were summed in SPC mode to provide an integrated frame. The sharpness of the emission image is limited by the collimator resolution and could be improved by optimized collimator design. We demonstrate that the same MAF is capable of operating in both SPC and EI modes and can be used in both X-ray transmission imaging and radionuclide emission imaging.**

Manuscript received October 06, 2011; revised March 13, 2012; accepted April 25, 2012. This work was supported by the NIH under Grants R01 EB002873 and EB008425.

A. Jain, A. Panse, D. R. Bednarek, and S. Rudin are with the Toshiba Stroke Research Center, University at Buffalo, Buffalo, NY 14214 USA (e-mail: ajain6@buffalo.edu; apanse@buffalo.edu; bednarek@buffalo.edu; srudin@buffalo.edu).

R. Yao is with the Department of Nuclear Medicine, University at Buffalo, Buffalo, NY 14214 USA (e-mail: rutaoyao@buffalo.edu).

Color versions of one or more of the figures in this paper are available online at http://ieeexplore.ieee.org.

Digital Object Identifier 10.1109/TNS.2012.2198493

***Index Terms*—Digital imaging, micro-angiographic fluoroscope (MAF), single-photon counting (SPC), X-ray imaging.**

I. Introduction

X-RAY and radionuclide imaging are among the most powerful imaging techniques in the medical imaging field. Normally in X-ray imaging, the prevailing mode of image acquisition is energy integrating (EI) mode, while single-photon counting (SPC) mode is more important for radionuclide imaging. In EI mode, the total energy deposited by photons is integrated to form the image. The digital number of any pixel in the image represents the amount of energy deposited at that particular location. Improvements in spatial and contrast resolution could be achieved with an alternative mode of imaging, the SPC mode [1]–[9]. In this mode, although light from a single event may spread across adjacent pixels, only one pixel in the cluster is selected as representing the detection location. Thus, an individual X-ray photon is counted, and the digital number at any pixel in the image represents the number of X-ray photons absorbed at that location. In energy integrating mode, detectors can show very high spatial resolution, but often are limited by the blur of the fluorescent phosphor. In comparison to EI mode, SPC mode shows better spatial resolution because the position of the event can be localized, and this minimizes the blur associated with conversion to secondary quanta. Others have also shown the improvement of spatial resolution with SPC mode [2]–[9]. Improved performance with better spatial and contrast resolution is gaining popularity for single-photon counting imaging over conventional imaging [2].

The newly developed high-resolution micro-angiographic fluoroscope (MAF) [10]–[12] has demonstrated superior clinical imaging capabilities. The heart of the MAF is the light image intensifier (LII) that enables the MAF to exhibit large variable gain. This large variable gain provides quantum-limited operation with effectively no additive instrumentation noise [12], [13]. The MAF is currently being evaluated as an EI X-ray transmission imager in a local hospital and providing encouraging results [10]. The dual mode of operation will make it more versatile. Others [3], [7] have shown SPC mode operation using an EMCCD that has an amplification stage in the CCD chip via an additional electron multiplying register. We will show the unique quality of the MAF detector operating

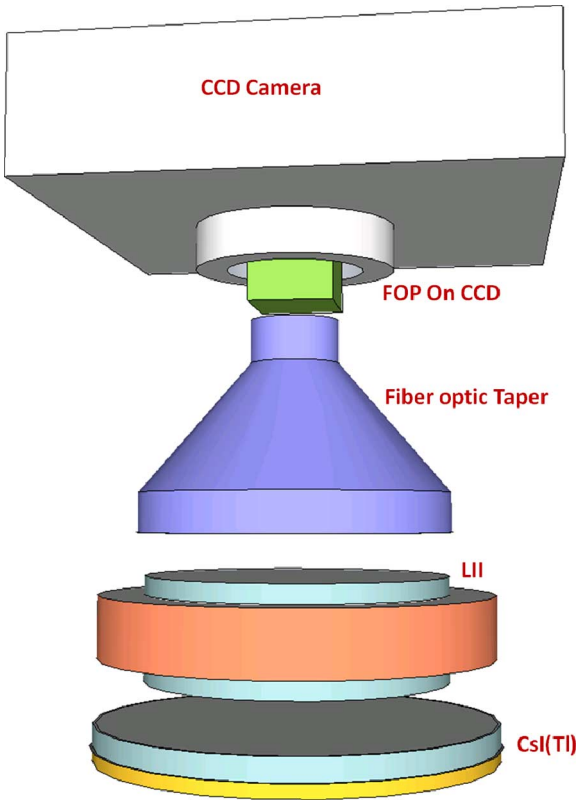

Fig. 1. MAF schematic (all components are contiguous).

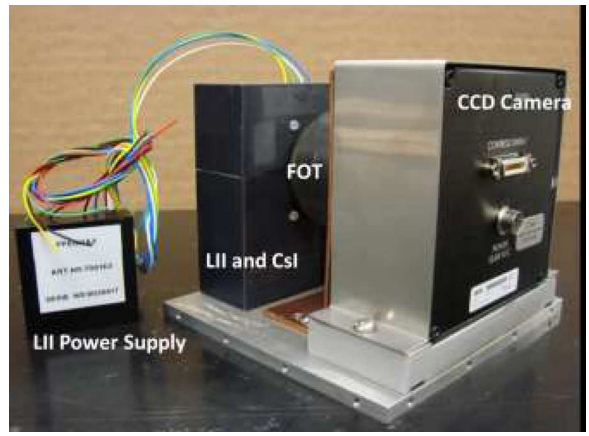

Fig. 2. Microangiographic fluoroscope.

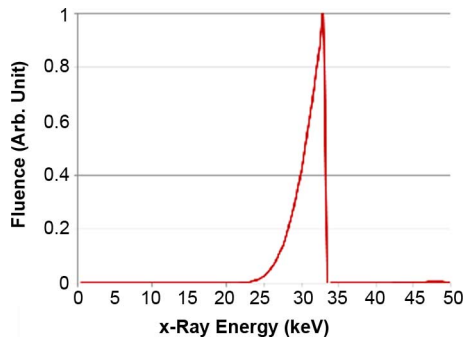

Fig. 3. Spectrum used for X-ray imaging in SPC mode.

in both EI and SPC modes and will compare the performance of the MAF in terms of spatial and contrast resolution in the two different modes of operation.

II. Method and Materials

A. Micro-Angiographic Fluoroscope

The MAF detector schematically shown in Fig. 1 and described extensively elsewhere [12] was used for this study. The MAF is a region of interest X-ray imaging detector capable of real-time imaging (30 fps) for both fluoroscopy and angiographic applications. The effective pixel size of the MAF of 35 μm provides very high spatial resolution.

As shown in Fig. 1, there is a CCD camera (DALSA 1M30, DALSA Corporation, Waterloo, ON, Canada) [14] coupled to a generation-2 dual micro-channel plate (MCP) light image intensifier (Model PP0410K, Delft Electronic Products B.V., Roden, The Netherlands) [15] through a 2.88-ratio fiber optic taper. The LII is coupled to a 300-μm-thick CsI(Tl) scintillator [16] through a fiber optic plate. A photograph of the MAF is shown in Fig. 2, and its specifications are given in Table I.

B. X-Ray Spectrum

For the transmission imaging SPC mode, we used an approximately monochromatic X-ray spectrum to improve the thresholding effectiveness. This spectrum was generated by adding 15 mm of iodine contrast media (density 350 mg/ml) as additional filtration to a 50-kVp X-ray beam from a clinical c-arm system (Infinix, Toshiba Medical Systems Corporation, Tustin, CA). The shape of the spectrum is shown in Fig. 3 as calculated using the SRS-78 X-ray spectrum generation software [17].

TABLE I
MAF Specifications

Scintillator	CsI(Tl)
CsI Thickness	300 micron
Field of view (FOV)	3.6 cm X 3.6 cm
FOT Ratio	2.88:1
Pixel Width	35 micron
Image Matrix	1024 X 1024
Light Image Intensifier	GEN 2 Dual MCP
Frame rate	30 fps
CCD Sensitivity	40 DN/(nJ/cm^2)
LII Gain SPC mode	~9000 ph/ph
LII Gain EI mode (fig. 17)	~500 ph/ph

C. Spatial Resolution and Contrast Studies

For a spatial resolution comparison of the SPC and EI modes used with X-ray transmission imaging, the MTF was determined using the standard slit method [18] and a mammographic line-pair phantom (line-pair range: from 5 to 20 lp/mm) was imaged for both modes. Additionally, a qualitative comparison of contrast between the two modes was made by imaging human distal and middle phalanges bones of the pinky finger from a hand skeleton embedded in plastic (not shown), which is illustrated diagrammatically in the right side of Fig. 4.

D. Phantom and Collimator for Radionuclide Imaging

The phantom used for the evaluation of the SPC emission imaging mode was a hot-rod phantom as shown in Fig. 5, where

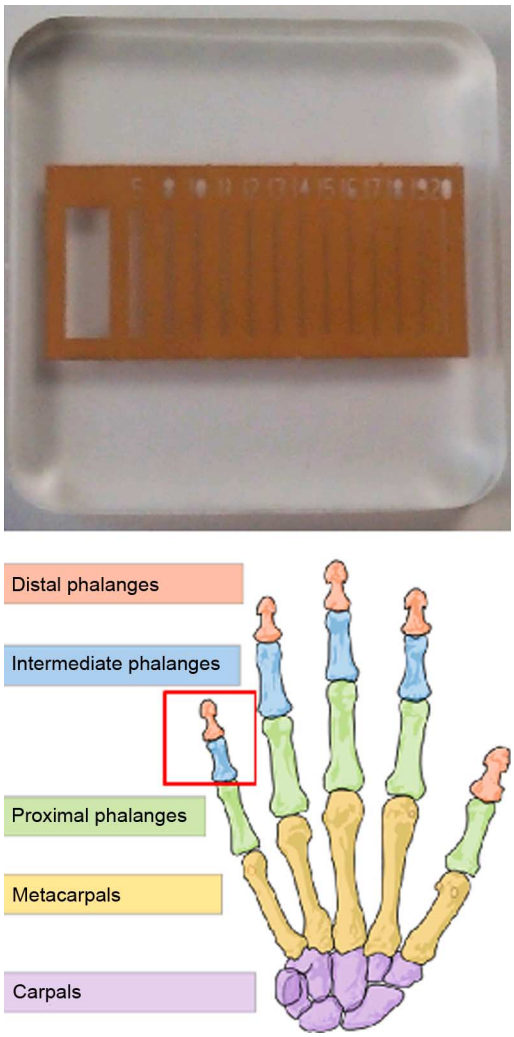

Fig. 4. Mammographic line-pair phantom and human phalanges bones used for spatial resolution and contrast evaluation.

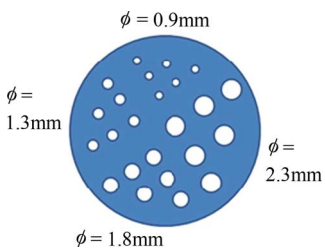

Fig. 5. Custom phantom designed for the SPC radionuclide imaging experiment.

the white circles represent cylindrical cavities in a plastic insert shown as solid color. This insert is placed in a cylindrical container that is filled with a solution containing 1 mCi of ^{125}I. The diameter of the phantom is about 3.5 cm. The depth of the hot rods is about 2 cm.

We used a medium-energy parallel-hole gamma camera collimator with lead septa and holes of 1 mm diameter and 24.5 mm height that was available to us. The CsI in the MAF was about 10 mm from the outer surface of the collimator, so the estimated collimator resolution was 1.24 mm for an object at its surface.

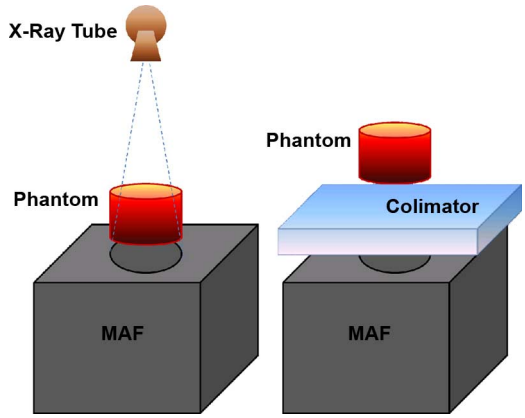

Fig. 6. Experimental set up diagram for *(left)* X-ray and *(right)* radionuclide imaging.

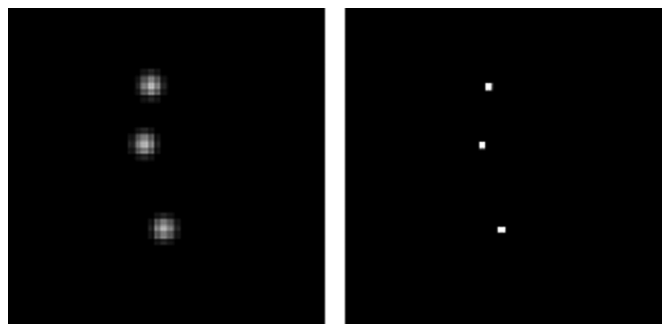

Fig. 7. Demonstration of simple thresholding technique. *(left)* Single frame slit image before thresholding. *(right)* Image after thresholding.

E. Setup for Experiments

For X-ray imaging in both modes, no gamma-camera collimator was used, and the phantoms were placed near the detector as shown in Fig. 6. The emission images were acquired by placing the collimator between the phantom and the MAF as shown in Fig. 6. The collimator was moved randomly during the acquisition to blur the collimator pattern.

F. Image Processing for Single-Photon Counting

For the image formation in SPC mode, the main task was to identify the events. For this preliminary study, basic threshold technique was applied. Photon absorption events were identified by using a threshold so that only those events above the selected threshold were registered. This effectively truncated the tails of the phosphor blur function. Afterward, the final image was formed by adding all events above the threshold from all the frames. In the thresholding technique, all the digital numbers below a threshold were considered zero, and all the digital numbers above that threshold were considered one (indicating a single event). Fig. 7 shows a demonstration of a simple thresholding technique on a simulated image.

For this technique, a threshold for the SPC mode was chosen so that the average fluence rate for accepted events corresponded to the estimated theoretical fluence rate determined using exposure measurements, the calculated X-ray spectrum, and absorption characteristics of the converting phosphor.

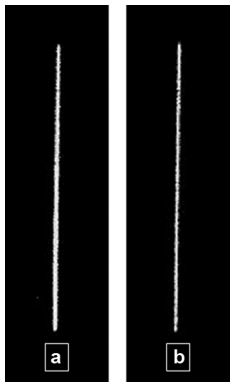

Fig. 8. Slit images for (a) energy integrating mode and (b) single-photon counting mode.

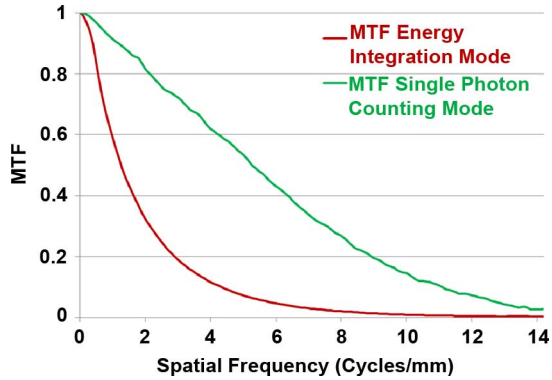

Fig. 9. Comparison of MTFs for both the EI and the SPC modes.

TABLE II
X-RAY PHOTON CALCULATIONS

No. of incident x-ray photons /mm^2 /μR	= 137
No. of incident x-ray photons /pixel /μR	= 0.17
Exposure per frame (μR)	= 1.37
No. of incident x-ray photons/pixel per frame	= 0.23
Absorption efficiency of CsI	= 0.67
No. of absorbed x-ray photons/pixel per frame	= 0.15
Slit Length (pixels)	= 244
Slit Width (pixel)	= 1/3
Slit Width (μm)	= 12
No. of photons per frame for slit area	= 10.98
No. of frames used for slit image	= 1200
Frame rate (per second)	= 20
SPC acquisition time (s)	= 60
Expected total counts	= 13176

This threshold level then provides an average of one count per X-ray photon absorbed. After getting a large number of thresholded images, we stacked them together to get a final composite image. All the images for the SPC mode for this study were processed similarly. For comparison, images were also obtained in EI mode using an exposure per frame equal to the total exposure for all SPC frames. In this way, we compared images from the two modes with the same total detector entrance exposure.

III. RESULTS

A. X-Ray Imaging in EI and SPC Mode

Table II shows some of the calculations used to determine the number of absorbed X-ray photons and the total counts expected. It shows that for the spectrum, the scintillator absorption efficiency, and the exposure (1.37 μR/frame) used, we expected to get an average of 0.15 absorbed X-ray photons per pixel per frame. We also have an example calculation for the slit image. Knowing the slit area, we calculated the number of X-ray photons per frame for the slit image. Once we knew that number, we applied the appropriate threshold to get the approximate count number to be close to the calculated one, and then we summed the frames and formed the SPC mode image.

Fig. 8 shows the comparison of the slit images taken in energy integrating and single-photon counting modes, respectively.

These slit images were used to calculate the modulation transfer function (MTF) using the standard slanted slit method [18]. Fig. 9 shows a comparison of the MTF for both modes and clearly demonstrates a substantial improvement with the SPC mode.

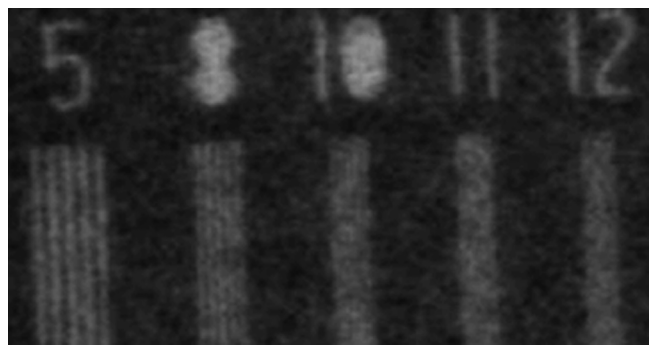

Fig. 10. Mammographic line-pair phantom images obtained with EI mode.

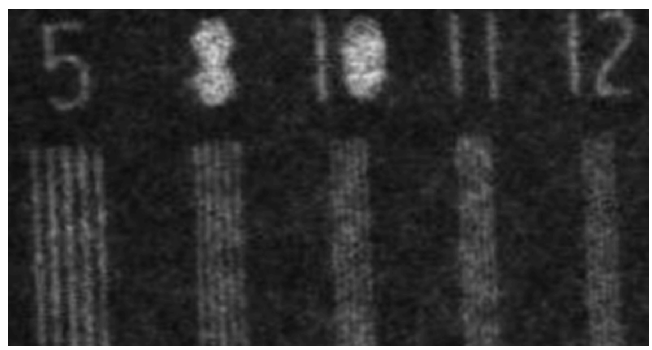

Fig. 11. Mammographic line-pair phantom images obtained with SPC mode.

The threshold selected for the slit images was applied to form the SPC image of the line-pair phantom and the human phalanges bones. The images of a mammographic line-pair phantom (Figs. 10 and 11) give a visual demonstration of the improvement in spatial resolution for the SPC mode over EI mode.

Figs. 12 and 13 show images of the human phalanges bone taken with EI and SPC modes. These images gave a visual demonstration of the contrast improvement with SPC mode over EI mode.

Fig. 14 shows normalized line profiles taken over the same selected region for the two different modes [indicated by the dotted arrows shown in the bone images (Fig. 14)]. For these phalanges bone images, 2000 frames were used for the image

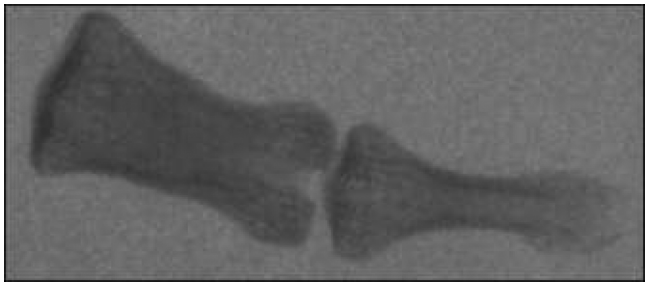

Fig. 12. Human phalanges bone images taken with EI mode.

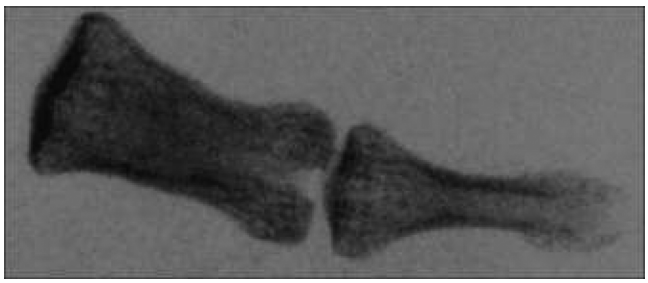

Fig. 13. Human phalanges bone images taken with SPC mode.

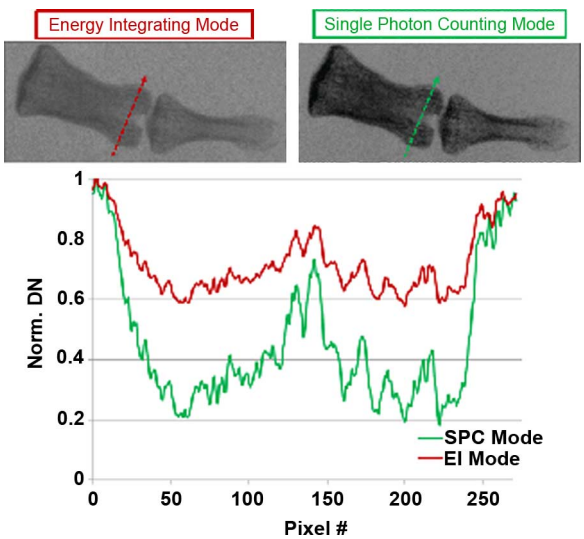

Fig. 14. Comparison of contrast details in human phalanges bone images. Normalized line profiles over the same selected region for the two different modes indicating the superior performance of the SPC mode.

formation in both the modes (EI and SPC) with the same exposure per frame used for the slit images $(1.37\ \mu\text{R/frame})$.

B. Radionuclide Imaging

The average energy of the X-ray spectrum and the emission from I-125 was close, and we were able to use the same threshold for the image formation in SPC mode with I-125. The image shown in Fig. 15 was generated by processing frames acquired in SPC mode for the radionuclide phantom keeping the collimator stationary. The hexagonal pattern corresponds to the collimator pattern. In Fig. 15, the collimator septa look brighter than the collimator hole. In our experimental setup, there is a nonzero distance between collimator and the detector,

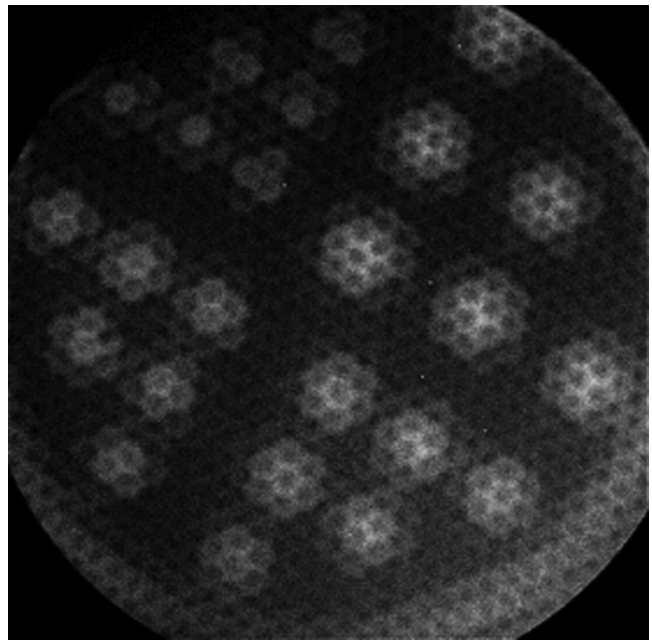

Fig. 15. Image of the radionuclide phantom generated in SPC mode from frames acquired with a stationary collimator.

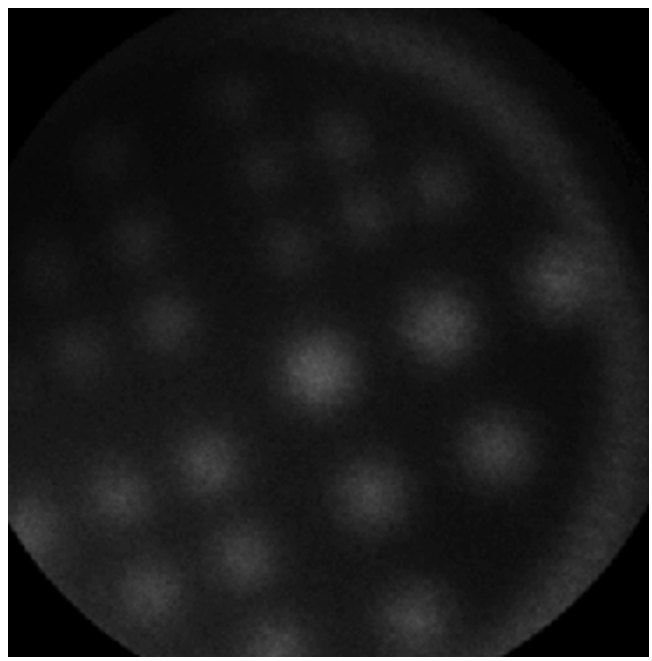

Fig. 16. Image of the radionuclide phantom generated in SPC mode from frames acquired with a randomly moving collimator.

and because of this nonzero distance, the event profiles from the adjacent collimator holes overlap and give a higher count in the septal region. If the collimator and detector were in contact, we would get a defined shadow of the septa with no overlap or enhanced brightness present. To eliminate this pattern, the collimator was moved in random directions, and the corresponding image is shown in Fig. 16. An X-ray transmission image of the same phantom is also shown in Fig. 17. The X-ray transmission image looks blotchy because the phantom was enclosed in layers of plastic and absorbent paper and sealed

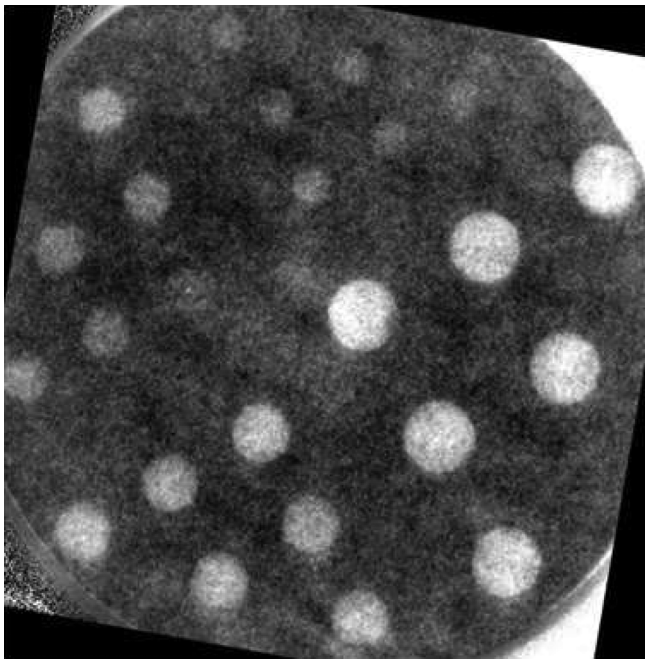

Fig. 17. Transmission X-ray image of the radionuclide phantom acquired by the MAF.

with fiberglass-reinforced sealing tape to contain any potential leak.

IV. Summary and Discussion

The slit image taken with SPC mode shown in Fig. 8 is visually sharper than the image taken in EI mode, while the experimentally derived MTF shows a dramatic improvement for the SPC mode over the EI mode at all frequencies as seen in Fig. 9. The improvement in MTF occurs because of the improved localization of events enabled by reducing the effect of light spreading and limiting detection to a single pixel. Images of the line-pair phantom shown in Figs. 10 and 11 also clearly demonstrate the resolution improvement by enabling visualization of groups at and above 10 lp/mm in SPC mode as well as improved contrast signal at all line-pair frequencies, even for the lower ones.

Another demonstration was related to qualitative contrast improvement. Figs. 12 and 13 showed images of the distal and intermediate human phalanges bones for both modes taken at an equivalent exposure. Bone details such as fine trabeculae were better visualized. For a quantitative contrast comparison, we took a line profile of the same region in both images and normalized it to the background levels. In this comparison of the line profiles in Fig. 14, we observed higher contrast for the finer details with SPC mode.

Successful performance of the MAF was demonstrated in both SPC and EI modes for X-rays. The same SPC mode was used to image a radionuclide phantom using the MAF. We were able to identify each hot rod in the phantom for both modes (Figs. 16 and 17) of imaging. The collimator pattern was removed by randomly moving the collimator during acquisition. As in scintillation camera imaging, emission imaging performance is currently limited by the collimator resolution, which is larger than 1.24 mm. This paper provides the proof of concept that the MAF can be used for both emission and transmission imaging. An improved collimator design should be able to greatly improve the spatial resolution for the MAF in radionuclide imaging.

In this study, we used quasi-monochromatic spectra because we were using a simple threshold technique to detect events. Better and more complex techniques (such as centroid detection) can be used to detect the event more accurately while retaining the energy information [3]–[5]. With those techniques, polychromatic spectra can be used. Nevertheless, at this stage the simple thresholding technique prevents the spectral analysis needed to discriminate against scattered photons, and hence the demonstration was limited to small subjects. Extrapolation to large animals and even humans would require such improved scatter elimination techniques to be developed.

Another issue of concern may be acquisition time. For this study, we used only 20 fps for acquisition, and hence this demonstration was aimed at static imaging applications where low count rates might be acceptable. However, the time required for acquisition can be made shorter if we were to use a higher fluence rate enabled by the use of a higher frame rate and/or smaller pixels with high speed CCDs.

Currently, this application is limited to low-energy isotopes such as I-125. If we replace the 300-μm-thick CsI with a 1000-μm-thick CsI, we would be able to achieve better absorption efficiency for higher-energy isotopes like Tc-99 m. The drawback of replacing the scintillator with a thicker one is of course loss in the X-ray imaging resolution performance. For applications where the resolution requirement for X-ray imaging is not critical and absorption efficiency for emission imaging is important, this thicker phosphor may be merited. For the radionuclide imaging, the height of the phantom will play an important role.

V. Conclusion

The work presented here clearly demonstrated the unique imaging capability of the MAF in both EI and SPC modes. It has been shown that the operation of the MAF in SPC mode provides both higher spatial resolution and better contrast that can be advantageous for demanding applications.

Successful operation of the MAF in both SPC and EI modes may also provide a potentially attractive detector for dual imaging applications such as combined nuclear medicine emission and X-ray transmission imaging with a single detector.

References

[1] A. Jain, A. Kulhs-Gilcrist, D. R. Bednarek, and S. Rudin, "Improved contrast and spatial resolution with single photon counting (SPC) for an area X-ray imager, the newly developed high-resolution micro-angiographic fluoroscopic (MAF) detector," in *Proc. IEEE Nucl. Sci. Symp. Med. Imag. Conf.*, Orlando, FL, Oct. 25–31, 2009, pp. 3012–3016.

[2] S. R. Amendolia, M. G. Bisogni, P. Delogu, M. E. Fantacci, G. Paternoster, V. Rosso, and A. Stefanini, "Characterization of a mammographic system based on single photon counting pixel arrays coupled to GaAs X-ray detectors," *Med. Phys.*, vol. 36, no. 4, pp. 1330–9, 2009.

[3] F. J. Beekman and G. A. de Vree, "Photon-counting versus an integrating CCD-based gamma camera: Important consequences for spatial resolution," *Phys. Med. Biol.*, vol. 50, pp. N109–N119, 2005.

[4] B. W. Miller, H. B. Barber, H. H. Barrett, I. Shestakova, B. Singh, and V. V. Nagarkar, "Single-photon spatial and energy resolution enhancement of columnar CsI(Tl)/EMCCD gamma camera using maximum-likelihood estimation," *Proc. SPIE*, vol. 6142, p. 61421T-1, 2006.

[5] B. W. Miller, H. B. Barber, H. H. Barrett, L. Chen, and S. J. Taylor, "Photon-counting gamma camera based on columnar CsI(Tl) optically coupled to a back illuminated CCD," *Proc. SPIE*, vol. 6510, p. 65100N, 2007.

[6] B. W. Miller, H. B. Barber, H. H. Barrett, D. W. Wilson, and L. Chen, "A low-cost approach to high resolution, single-photon imaging using columnar scintillators and image intensifiers," in *Proc. IEEE Nucl. Sci. Symp.*, Nov. 1, 2006, vol. 6, pp. 3540–45.

[7] T. C. Soesbe, M. A. Lewis, N. V. Slavine, E. Richer, F. J. Bonte, and P. Antich, "High-resolution photon counting using a lens-coupled EMCCD gamma camera," *IEEE Trans. Nucl. Sci.*, vol. 57, no. 3, pp. 958–963, Jun. 2010.

[8] L. J. Meng and G. Fu, "Investigation of the intrinsic spatial resolution of an intensified EMCCD scintillation camera," *IEEE Trans. Nucl. Sci.*, vol. 55, no. 5, pp. 2508–2517, Oct. 2008.

[9] B. W. Miller, H. H. Barrett, L. R. Furenlid, H. B. Barber, and R. J. Hunter, "Recent advances in bazookaspect: Real time data processing and the development of a gamma-ray microscope," *Nucl. Instrum. Methods Phys. Res. A*, vol. 591, no. 1, p. 272, 2008.

[10] M. J. Binning, D. Orion, P. Yashar, S. Webb, C. N. Ionita, A. Jain, S. Rudin, L. N. Hopkins, A. H. Siddiqui, and E. I. Levy, "Use of the micro-angiographic fluoroscope for coiling of intracranial aneurysms," *Neurosurgery*, vol. 69, no. 5, pp. 1131–1138, Nov. 2011.

[11] P. Kan, P. Yashar, C. N. Ionita, A. Jain, S. Rudin, E. L. Levy, and A. H. Siddiqui, "Endovascular coil embolization of a very small ruptured aneurysm using a novel microangiographic technique," *J. Neurointerv. Surg.*, 2012, DOI: 10.1136/neurintsurg-2011-010154, Tech. Note, unpublished.

[12] A. Jain, D. R. Bednarek, C. Ionita, and S. Rudin, "A theoretical and experimental evaluation of the micro-angiographic fluoroscope (MAF): A high resolution region-of-interest X-ray imager," *Med. Phys.*, vol. 38, no. 7, pp. 4112–4126, 2011.

[13] G. K. Yadava, A. T. Kuhls-Gilcrist, S. Rudin, V. K. Patel, K. R. Hoffmann, and D. R. Bednarek, "A practical exposure-equivalent metric for instrumentation noise in X-ray imaging systems," *Phys. Med. Biol.*, vol. 53, no. 18, pp. 5107–21, 2008.

[14] Philips Semiconductors, Eindhoven, The Netherlands, "FTT1010-M frame transfer CCD image sensor," Datasheet, 1999.

[15] Delt Electronic Products B. V., Roden, The Netherlands, "Image intensifier tube brochure," 2007.

[16] Hamamatsu Corp., Bridgewater, NJ, "FOS—Fiber optic plate with scintillator for digital X-ray imaging," 1996.

[17] K. Cranley, B. J. Gilmore, G. W. A. Fogarty, and L. Desponds, "Catalogue of diagnostic X-ray spectra and other data," Inst. Phys. Eng. Med., Rep. No. 78, 1997.

[18] H. Fujita, D. Y. Tsai, T. Itoh, K. Doi, J. Mrishita, K. Ueda, and A. Ohtsuka, "A simple method for determining the modulation transfer function in digital radiography," *IEEE Trans. Med. Imag.*, vol. 11, no. 1, pp. 34–39, Mar. 1992.